AIAA Propulsion and Energy Forum
19-22 August 2019, Indianapolis, IN
AIAA Propulsion and Energy 2019 Forum

10.2514/6.2019-4187

Development and Preliminary Testing of Paraffin Hybrid Rocket Fuel Grains with Helical Port Structures

Lucas LB. Pabarcius*
Wesleyan University, Middletown, Connecticut, 06459, USA

This paper proposes the use of helical ports as a means of improving the current upper limit of reported hybrid rocket regression rates and therefore the range of potential hybrid rocket applications. An accessible, low-cost method of producing paraffin-based hybrid rocket fuel grains for lab-scale use is demonstrated, whereby vacuum degassed, blackened paraffin is cast into a range of additively manufactured acrylonitrile-butadiene-styrene (ABS) molds. A test system and gaseous oxygen fed hybrid rocket motor has been developed to test the resultant fuel grains. Preliminary results are reported for cast paraffin and ABS fuel grains, including reconstructed regression-time histories and hot-fire observations. Further combinations of paraffin fuels and additive manufacturing processes are proposed.

I. Nomenclature

A_{inj}	=	injector throat area, m 2	R_u	=	universal gas constant, J/mol/K
t	=	time, s	M	=	molecular weight, kg/mol
$\dot{r}$	=	fuel regression rate, m/s	G_{ox}	=	oxidiser mass flux, kg/m^2-sec
L	=	grain length, m	c^*_{theo}, c^*_{actual}	=	characteristic velocity, m/s
L^*	=	characteristic length, m	C_d	=	discharge coefficient
P_{inj}. P_c	=	upstream and chamber pressure, bar	$\dot{m}_f$, $\dot{m}_{ox}$,	=	fuel and oxidiser mass flow rate, g/s
γ	=	isentropic exponent	η_c	=	combustion efficiency
r	=	radius, m	N	=	number of rotations
m	=	mass, kg	ρ	=	density, kg/m^2
Φ	=	pitch ratio, unitless	T	=	temperature, K

II. Introduction

A. Advantages

HYBRID rocket motors potentially offer an assortment of advantages when compared with their liquid and solid counterparts, including simplified throttling, reduced cost, and improved safety [1]. Their plumbing could utilize half as many components as equivalent liquid fuel systems, while avoiding hard starts and transport hazards. Interest has recently grown in improving hybrid motors' Technology Readiness Level (TRL) due to their promise as "market disruptive" [2] satellite and CubeSat boosters in the range of 20–100N [2-4]. At a larger scale, the current development of the hybrid Mars Ascent Vehicle (MAV) system is actively improving hybrid TRLs. A key uncertainty in the performance of paraffin fuels was resolved this past year, as both 80 and 90 s burns were separately demonstrated [5] [6] using novel oxidizers such as MON-3 and HTP. Although implementation barriers are higher at larger scales, trade studies show promise for upper stage hybrids, with up to 40% payload increase predicted for motors impulse-matched to Orion 38 [7]. Finally, other efforts have recently developed novel hybrid ignition methods, including hypergolic, laser, and electrical arc-based techniques [3, 8-11].

* Student, Physics, AIAA Member.

B. Outlook

Five key factors of space-access are cost, safety, simplicity, reliability, and environmental impact [12]. Each can potentially be improved upon with an effective hybrid system. The costs of preliminary launch systems are a key hurdle for new launch providers and emerging nations beginning to develop their space program. If successful development of satellite hybrid propulsion systems is achieved, the improved characterization and understanding of hybrid systems involved could create a cascade of applications with increasing scale, therefore increasing access to space. As scale and L^* increase, so will combustion efficiency, which is often a weak performance parameter [13]. If this occurs, regression rates will likely remain the primary factor limiting broad adoption. In 1997, a progress report from researchers at Pratt and Whitney indicated that the use of hybrid rocket motors in early launch stages would ideally involve creating a 12x improvement over standard HTPB regression rates when compared with the low L/D ratio Castor-120 motor [14]. Current efforts range from a well-characterized 3x improvement over standard HTPB systems, seen with paraffin fuels, helical ports, and swirl injection, to preliminary studies combining techniques with amplification factors up to 5x.

C. Research goals

This research intends to add to the body of similar work testing additively manufactured hybrid fuels at lab-scales, with the hope of demonstrating an applicable configuration for larger scale propulsion systems. I suggest that the increased skin friction and reduced radial blowing effect created by helical ports [15] will in turn increase droplet entrainment rates [16]. In addition, increased oxidizer turbulence and port residence times are predicted to improve combustion efficiency. Previous works involving paraffin and FDM manufactured plastic substrates have been attempted with variable success, finding incomplete combustion [17] and marginal regression rate enhancement [18]. This research aims to instead use the printed structure as an intermediate component of the paraffin grain manufacture process, allowing helical fuel grains to be produced without adding procedural complexity.

III. Method of Approach

D. Grain Production

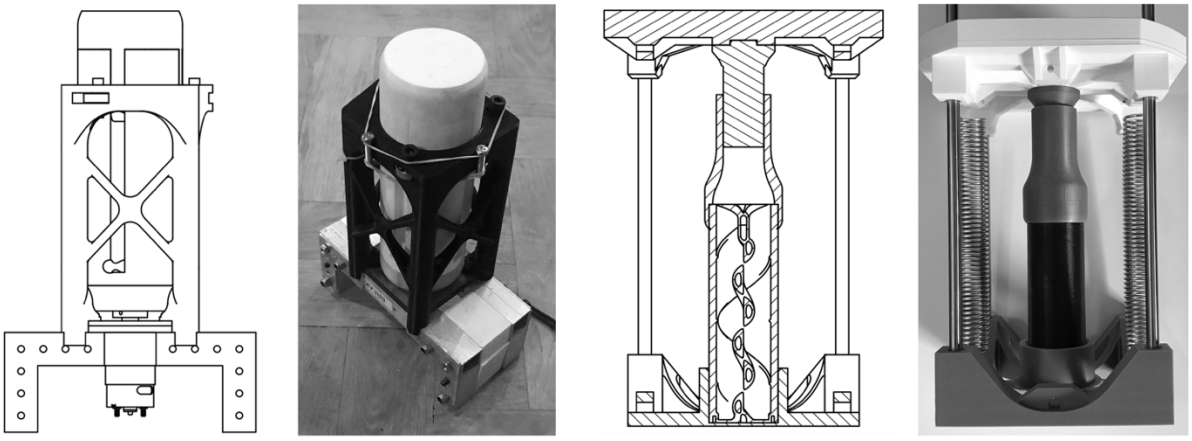

Fig. 1 (L) Centrifugal and (R) Plunger-Pressurized Casting Apparatus

Two casting methods were developed, centrifugal and plunger-based. Due to limited access to machining resources, both systems were largely produced using FDM processes, demonstrating the technologies' versatility and accessibility in producing specialized systems. A vertical centrifuge capable of sustained spinning at 800 RPM was created. Although centrifugal casting is a well-established technique [19], the apparatus produced a visible gradient of carbon black density and inconsistent voids along the central axis of high pitch helical grains. An alternate plunger-operated system was built, based on the technique proposed and used by Bernard Geneviève in the UKZN hybrid sounding rocket program [20]. Calibrated springs were used to provide constant pressure on the wax as it cooled while accommodating wax shrinkage. A pressure of 5 bar (abs.) was chosen to limit the risk of damaging plastic components.

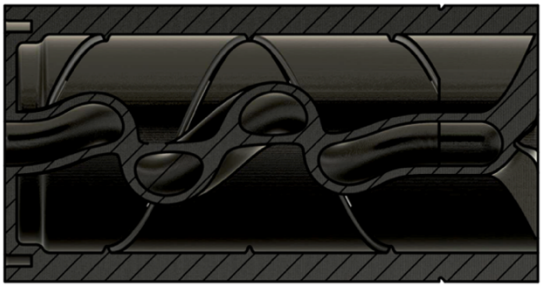

Fig. 2 CAD Model of Short Configuration Fuel Grain Mold

ABS exhibits a glass transition at 105ºC, whereas the paraffin wax used, Kerax® 1303, was seen to melt between 74ºC and 76ºC via ASTM D 127. This discrepancy allowed for paraffin to be cast into ABS molds. Molds were modeled in Autodesk® Fusion 360™ and printed with a Prusa MK3 i3 desktop printer. As injector and pre-combustion chamber flow patterns have been demonstrated to have substantial impact on observed regression rates [21], the helix was modelled with centered and axially aligned fore and aft ports. The 'smoothest' radial scaling function with this characteristic was selected on the basis of the maximum port diameter that did not return self-intersection errors. Added design features included a temporary upper section to support and seal the port during casting, counter-rotating ridges along the inner mold surface to prevent paraffin debonding, and pre-combustion chamber alignment inserts. The high pitch ratio, short configuration design is shown in Fig. 2.

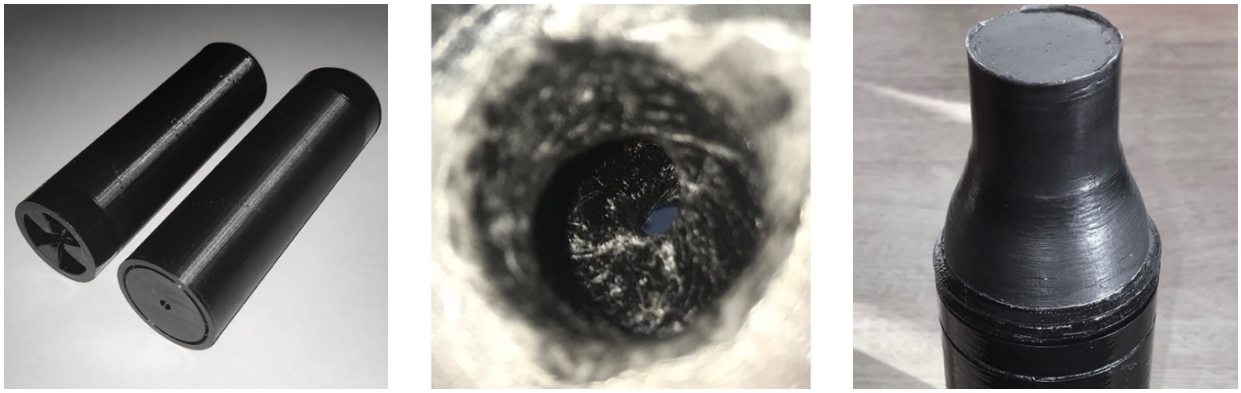

a) **b)** **c)**

Fig. 3 Helical and Straight Port Molds (a). Final Helical Paraffin Port (b). Excess Post-Cast Wax Section (c)

To ensure ABS molds were pressure tight, 10 ml of acetone-ABS slurry was poured into the casting void and vigorously shaken. Kerax 1303 paraffin was mixed with 1% carbon black, then melted and degassed in a commercial vacuum chamber for 15 minutes before being poured into casting molds. Plunger-pressurized casts were set to cool in an oven preheated to 85º C over 5 hours. Preliminary observations and dissection of fuel grains indicate high fidelity casts which even retain the printed molds' fine surface features. Although plunger casting at 10 bar has been demonstrated to produce adequately homogenous fuels [22], paraffin regression rates are remarkably variable between preparation process and composition, so more analytical assessment into the procedures' impact on material properties and viability at scale is necessary. After casting, the excess wax seen in Fig 3c is machined off to reveal the ABS-filled port. The central ABS mandrel was configured to be "burnable" as is, but was instead filled with acetone and dissolved to reduce uncertainty in firing results. The resultant port is shown in Fig. 3b.

As a means of initial assessment, radiographic scans were taken of a fuel grain which had been deliberately cast without plunger pressurization, seen in Fig. 4c. Additional scans were taken of helical test specimen 2-1 (Fig. 4a,b), revealing a well-preserved port structure. By comparison between the two samples, the process seems to mitigate against internal stress-fractures, though more validation is needed.

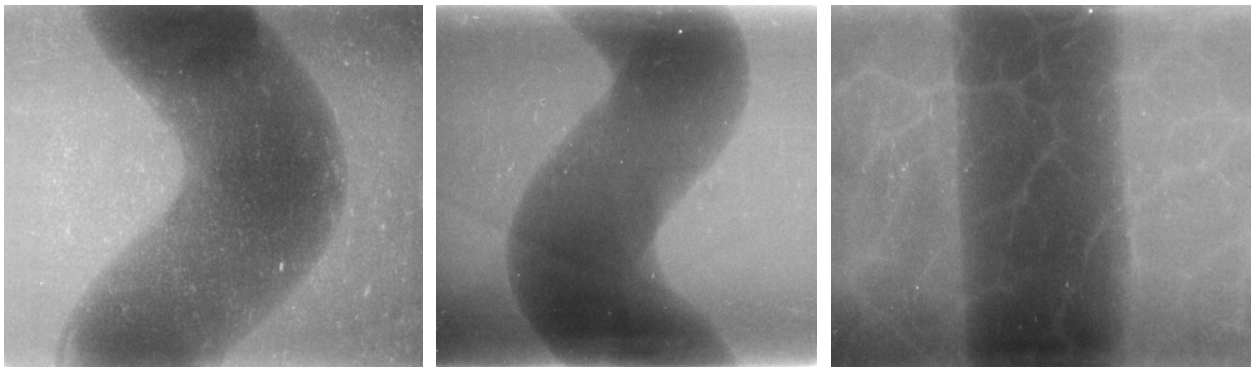

a) b) c)

Fig. 4 X-Ray Scans of Cast Helical Fuel Grains (a,b). Fuel Grain Cast Without Plunger Apparatus (c).

E. Helical Parameterization

$$K = \frac{2\pi N}{L} \quad (1)$$

$$R = Kr_{helix} \quad (2)$$

$$V = \pi r^2 L\sqrt{R^2 + 1} \quad (3)$$

$$(r_{port} - r_{helix}) = \frac{1}{KR} \quad (4)$$

Previous efforts into helical-port hybrid rockets have recognized a phenomenon in which tubular helixes 'coil up' and approach a cylindrical shape as their cross-sectional radius increases beyond a certain value [16]. This poses a challenge for designers of helical-port fuel grains, as it results in a non-computable CAD-model at the point where the parametric surface of a tubular helix begins to self-intersect- once Eq. 4 is satisfied. This restricts proper characterization of helical fuel characteristics for large aspect-ratio burns, as there is no known closed-form function for a self-intersecting helix's volume in terms of its radius. Further, the surface will continue to recursively self-intersect as the radius grows. The typical function for a helical volume is Eq. 3, defined by the product of port area and helical path length. To assess inaccuracy of this model in the domain of over expanded helical ports, a parametric solution for the cross-sectional border of a helix was calculated. The outermost intersection was numerically solved allowing for the creation of a discretized mesh surface in Mathematica whose area ($A_H(r_{port})$) is well defined for all port radii (Fig. 5). The helical volume can then be calculated by $L^*A_H(r_{port})$, which matches the value of Eq. 3 to within 0.1%

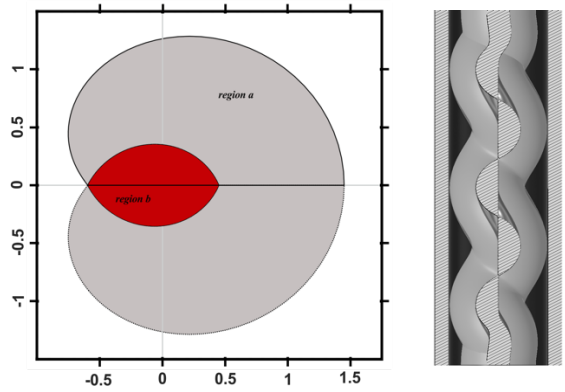

Fig. 5 Helical Cross-Section at r_{helix}= 1 (L) and CAD-Modeled Port Expansion (R)

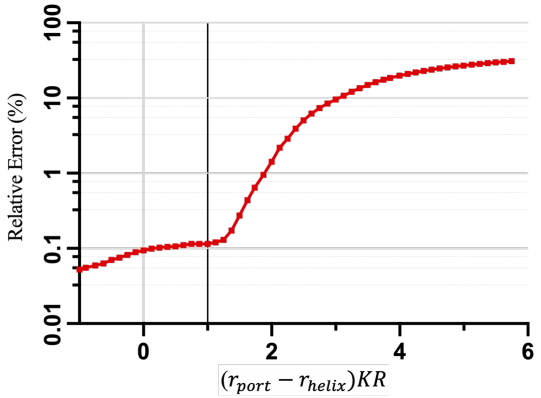

Fig. 6 Relative error of Helical Volume Calculated by Eq. 3 and Actual Volume (by Discretization)

(likely attributable to floating point and mesh errors) in the well-defined region. Relative error of the two methods is presented (Fig. 6) to demonstrate the domain under which computationally intensive mesh discretization may be avoided. Fortunately, the grains used in this study maintained radii with peak error < 3%, so Eq. 3 will be applied from this point onward.

F. Test System Development

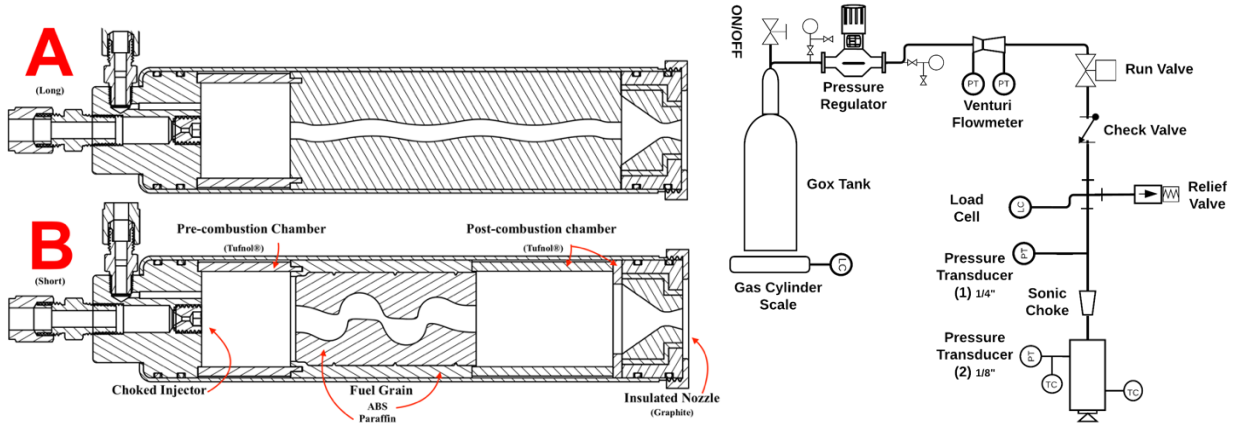

Fig. 7 (L) Lab Scale Motor Scheme and (R) Simplified P&ID of Preliminary Test System

An instrumented GOX-based test system and 40N hybrid rocket motor has been developed to characterize the 54mm diameter fuels. Nozzle and injector design specifications are optimised for 150psi chamber pressure. A choking injector was chosen to ensure a steady oxidizer mass flow rate and to decouple chamber instabilities. The orifice diameter was drilled to 1.6mm, with conical inlet to improve C_d and promote recirculation. To ensure the predicted low oxidiser to fuel ratios did not excessively affect performance and regression analysis, a shorter "B" grain configuration was produced, shown in Fig. 4. Manufacturing constraints lead to final selection of a COTS motor casing and enclosure (Pro54®-2G). Motor and test-stand design were based on the successful ProX® / flexural plate systems deployed by Whitmore et al at Utah State University [2, 3, 10].

$$\dot{m}_{ox} = C_d P_{inj} A_{inj} \sqrt{\frac{M\,\gamma}{T\,R_u}\left(\frac{2}{\gamma+1}\right)^{\frac{\gamma+1}{\gamma-1}}} \qquad (5)$$

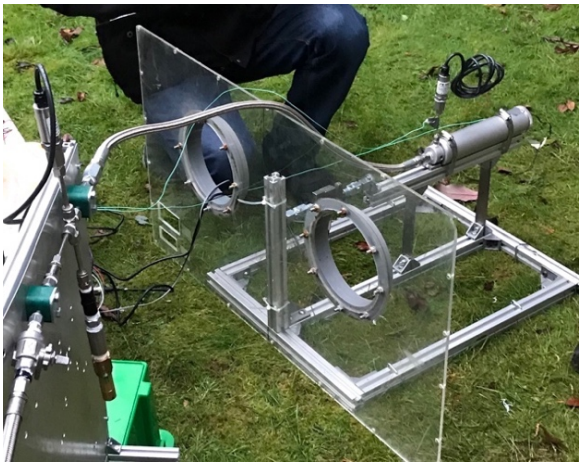

Fig. 8 Assembled Test System Pre-Firing

Measurement apparatus include OMEGA-PXM309 pressure transducers recording both upstream and chamber pressure, a 245N s-beam load cell for thrust, and type K thermocouples mounted on the chamber casing and pressure tap pipe. A custom venturi flow-meter was also built to aid calibration and regression rate reconstruction. In addition, thrust measurements were calibrated for losses from the test stand prior to each test campaign.

The test system is capable of oxidizer mass flow rates approximately ranging between 7.5 g/s and 20 g/s, depending on fuel configuration and desired thrust. The orifice and venturi flow-meter discharge coefficients were calibrated in cold flow tests using a gas cylinder scale and the one-dimensional equation for ideal choked flow, shown in Eq. 5.

IV.Preliminary Results and Discussion

G. Test Firings

Three test campaigns were successfully carried out between January and June 2019, producing workable sensor data and validating motor design and manufacture. Both a venturi and a pneumatic-cylinder operated run valve have been added to the test system following January testing and issues of upstream pressure droop and partial leakage from the system relief valve have since been resolved. The system is now producing remarkably clean pressure and thrust traces, as seen in Fig.10

Tests 0-0 and 0-1 were unable to be used for regression reconstruction as the ABS used in test 0-0 was found to have been printed at partial infill, and test 0-1 lacked accurate upstream pressure readings from which to derive oxygen mass flow.

Ongoing efforts in improving the test system will focus on replacing the current pyrotechnic ignition system and the addition of a nitrogen purge loop to prevent residual burning.

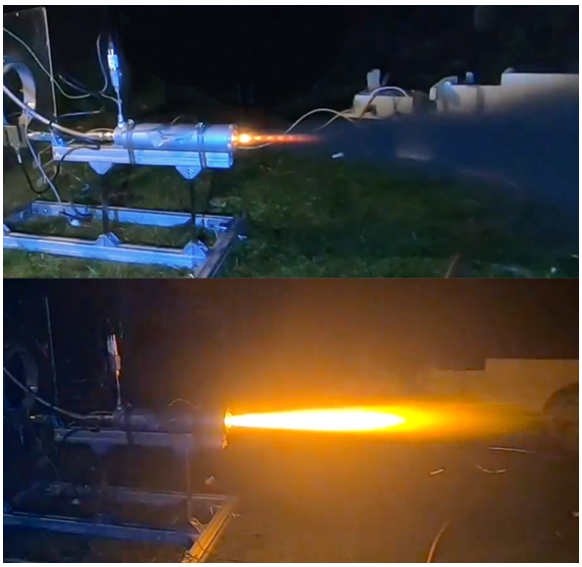

Fig. 9 Plume Variation in Straight Port Paraffin Hot-Fire 0-1

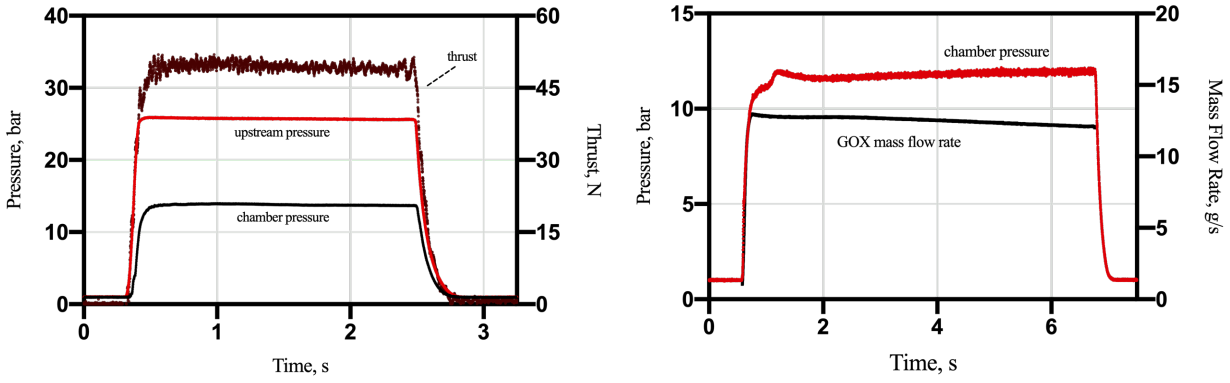

a) **b)**

Fig. 10 (a) Raw Upstream, Chamber Pressure, and Thrust Traces (test 2-3)**.**

(b) Chamber Pressure and Calculated Oxygen Mass Flow Rate (test 2-0).

Table 1. Test Measurements

Test	*L, cm*	r_i, *cm*	$\bar{P}_c$, *bar*	$\bar{F}_{thrust}$, *N*	Δm_f, *g*	$\bar{\dot{m}}_{ox}$, *g/s*	t_{burn}, *s* (30% $\bar{P}c$)	$N\, r_h / r_p$ Pitch Ratio, Φ	*Fuel Grain*
~~0-0~~	8.78	0.85	14.037	46.91	82.61	*oxidizer leak*	6.48	0	Paraffin
~~0-1~~	14.18	0.40	12.589	41.13	65.97	11.622	5.85	0	ABS*
1-0	13.53	0.425	11.159	36.76	83.45	11.957	4.10	1.5	Paraffin
~~1-1~~	14.22	0.452	*sensor failure*	42.49	112.39	12.163	12.99	3	ABS
2-0	14.221	0.453	11.569	39.80	48.38	12.487	6.29	0	ABS
2-1	7.995	0.465	12.477	43.56	26.32	13.061	1.46	3	Paraffin
2-2	7.921	0.471	9.587	33.24	34.31	10.792	3.18	0	Paraffin
2-3	7.699	0.568	13.208	46.60	35.63	13.411	2.26	2	Paraffin

a) **b)** **c)**

Fig. 11 Post-Burn Helical Port (b). Residual Paraffin Film in Pre-Combustion Chamber (a,c)

CFD modelling of conical axial injection schemes indicates significant pre- and post-combustion chamber recirculation patterns [21]. Fig. 11(b,c) shows a thin paraffin film that was found to coat the inner surfaces of the pre-combustion chamber, indicating a substantial recirculation zone and fuel mixing. However, a notable challenge for large scale paraffin-based hybrid rocket motors was also observed in post-test paraffin specimens, which began to pool liquid paraffin as heat radiated from the surrounding chamber after motor shutdown.

H. Equilibrium & Reconstruction

Chemical equilibrium calculations are an important part of both hybrid motor design and test analysis. They are made possible by understanding both fuel composition and formation enthalpy. Interpolation of reported alkane melt point values and corresponding carbon numbers resolved a mean paraffin composition of $C_{35}H_{72}$ [23]. By group addition the heat of formation was found to be *-1651.32 kJ/kg*. Previous work on ABS fuels has reported typical mole fractions of 50% butadiene, 43% acrylonitrile, and 7% styrene, with heat of formation = *-1097.42kJ/kg* [10].

$$\eta_c = \frac{c^*_{actual}}{c^*_{theo}} = \sqrt{\frac{Tactual}{T_{theo}}} \tag{6}$$

$$\bar{c}^* = \frac{\bar{A}^* \int P_c\, dt}{\int \dot{m}_{ox}\, dt + \Delta m_f} \tag{7}$$

$$\Delta m_f = \int \dot{m}_f dt = \int \frac{P_c \bar{A}^* - \eta_c \dot{m}_{ox}\, c^*_{theo}(P_c, OF\prime)}{\eta_c\, c^*_{theo}(P_c, OF\prime)}\, dt \tag{8}$$

In 1999, Wernimont et al [24] proposed a reconstruction technique to iteratively model scaled regression-time histories from chamber pressure traces and chemical equilibrium calculations. These techniques have since been improved on and made robust against non-convergence [25] [26]. Following from the arrangement used by Whitmore et al, three-dimensional tables of cubic-spline interpolated chemical equilibrium parameters have been prepared for the expected range of chamber pressures and O/F values using the opensource software ProPep. Computation follows the RT-5 routine developed by Saito et al [26], using chamber pressure traces and oxidizer mass flow rates calculated by Eq. 5. Eq. 8 is then iteratively computed at varying combustion efficiencies via Python, using the secant method to minimize error to 2e-8. Regression rate curves can also be OF-corrected via Eq. 11, derived in [27], though they are presented with the caveat that their space-averaging assumptions have not yet been assessed in helical domains.

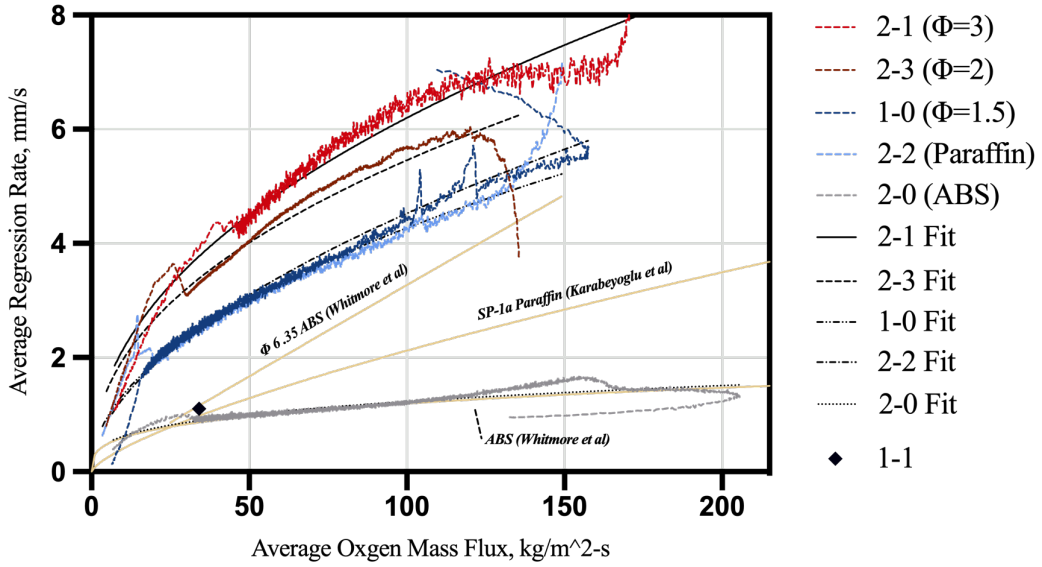

Fig. 12 Regression Rate for ABS, Paraffin, and Helical Grains (Without O/F Correction)

$$r_{port}(t) = \sqrt{r_i^2 + \int_0^t \frac{\dot{m}_f}{\rho \pi L} dt} \qquad (9)$$

$$r_{port\,H}(t) = \sqrt{r_i^2 + \int_0^t \frac{\dot{m}_f}{\rho \pi L \sqrt{R^2+1}} dt} \qquad (10)$$

$$\dot{r}(OF) = \dot{r}(OF') \frac{(1+OF\prime)(1-\left(\frac{OF\prime}{1+OF\prime}\right)^n)}{(1+OF)(1-\left(\frac{OF}{1+OF}\right)^n)} \qquad (11)$$

Reconstruction of radius-time histories from fuel mass flow was calculated using Eq's. 9 and 10. Eq. 10, derived from Eq. 3, was implemented for helical grains to more accurately reflect the component of oxygen mass flux that is tangential to the helical surface. However, empirical relationships are also presented using Eq. 9 for helical grains, as flow is anticipated to 'straighten out' as the port nears a cylinder. These two curves are expected to help provide a bound that will remain accurate for a larger range of scales, Reynolds numbers, and flow rates.

Table 2. Fitted $\dot{r} = aG_{ox}^n$ Relationships with Bootstrapped 95% Confidence Intervals

Fuel	*Φ*	*O/F avg*	a_{corr} *(OF = 2.0)*	*a (raw)*	*CI +*	*CI -*	*n*	*CI +*	*CI -*	*R^2*	η_{c^*}%
ABS	0	1.504	0.325	0.315	0.318	0.312	0.296	0.298	0.293	0.869	94
Paraffin	0	1.000	0.452	0.425	0.429	0.422	0.501	0.503	0.499	0.978	93
Paraffin	1.5	0.597	0.405	0.364	0.368	0.361	0.547	0.550	0.544	0.961	80
(Eq.10)			0.407	0.365	0.368	0.361	0.547	0.549	0.544	0.964	
(Eq.11)	2	0.851	0.772	0.707	0.719	0.695	0.444	0.448	0.440	0.933	96
Paraffin			0.728	0.667	0.686	0.668	0.453	0.456	0.450	0.960	
Paraffin	3	0.725	0.823	0.741	0.755	0.726	0.461	0.466	0.457	0.960	89
			0.828	0.745	0.757	0.733	0.458	0.462	0.454	0.967	

V.Conclusion

A versatile test system, motor, and casting procedure for small-scale helical paraffin fuel grains has been successfully developed. Preliminary GOX testing has demonstrated substantial regression rate amplification factors over ABS on the order of 6-7x, even at remarkably low O/F ratios. Regression rates have been presented using Saito et al's RT-5 reconstruction routine, with basic modifications made to account for helical port geometry. The exact relationship between pitch ratio and regression for non-thermoplastic fuels remains unclear, as well as why the paraffin used in this study started with such a remarkably high regression rate. Nonetheless, these results are promising for the field of non-standard hybrid fuels and specifically for those grains produced by additive processes which allow for greater tailoring and refinement of performance parameters than might be found with fuel composition alone.

Follow-on work will investigate helical grain production for higher O/F ratio mid-scale wax hybrids and semi-analytical modelling of burn behavior. Current print-bed limitations indicate a multi-segmented structure will be required if additively manufactured molds continue being used. Larger scale stacked paraffin slabs have shown promising results in hot-firings [28], indicating that this approach could be successful.

The ProJet HD3500 Multi Jet Modeling printer is an alternate manufacturing option, having successfully produced fuel grains composed of Visijet® S300 wax [29]. Three proposals are suggested for Multi Jet Modeled wax grains. First, the 'dry towel' channels used in end-burning hybrid rocket motors could be adapted for radial burning designs to either carry unburnt oxidizer into the post-combustion chamber, or be modified to produce vorticial flow along the fuel port [30] [31]. Finally, two separately characterized fuels can be combined with a variable local mixture ratio dependent on axial distance and radius, creating uniform longitudinal regression and minimizing O/F shift.

VI.Appendix

$$\vec{C}(t) = \{r_h\, cos(Kt)\,, r_h\, sin(Kt)\,, t\} \qquad (12)$$

$$\vec{N}(t) = \{-cos(Kt)\,, sin(Kt)\,, 0\} \qquad (13)$$

$$\vec{B}(t) = \left\{\frac{sin(Kt)}{\sqrt{R^2+1}}, \frac{-cos(Kt)}{\sqrt{R^2+1}}, \frac{R}{\sqrt{R^2+1}}\right\} \qquad (14)$$

$$\vec{H}(t, r_p, \varphi) = \vec{C} + r_p\, cos(\theta)\, \vec{N} + r_p sin(\theta)\, \vec{B} \qquad (15)$$

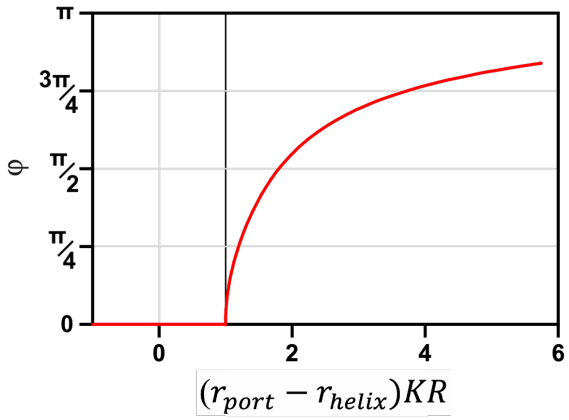

Fig. 13 Angular Deviation from Normal Vector to Outermost Helical Self-Intersection

$$\left\{\begin{array}{l} \left(r_h - r_p\, cos(\theta)\right) cos\left(\frac{-r_p KR sin(\theta)}{\sqrt{R^2+1}}\right) - \frac{r_p sin(\theta) sin\left(\frac{-r_p KR sin(\theta)}{\sqrt{R^2+1}}\right)}{\sqrt{R^2+1}}, \\ \left(r_p\, cos(\theta) - r_h\right) sin\left(\frac{-r_p KR sin(\theta)}{\sqrt{R^2+1}}\right) - \frac{r_p sin(\theta) cos\left(\frac{-r_p KR sin(\theta)}{\sqrt{R^2+1}}\right)}{\sqrt{R^2+1}} \end{array}\right\} = \vec{Q}\,,\ Zero(\vec{Q}y) \le \varphi \le 2\pi - Zero(\vec{Q}y) \qquad (16)$$

A helical surface may be parameterized by a coil (Eq. 12) and a circle drawn on the plane formed by its corresponding unit normal and binormal vectors. (Eq's 13,14). The intersection of this helical surface function (Eq. 15) with the x, y plane was found to produce a semi limaçon-shaped curve which is described by Eq. 16 and whose outermost boundary is shown in Fig. 5. The first intersection point of the helical surface was found to occur at the closest zero of the binormal (y) component of $\vec{Q}$ to $\theta = \pi, (\neq \pi)$ which was resolved with Newton's method using seed r_p (plotted in Fig. 13). Eq. 16 may then be made into a discretizable surface by parameterizing in terms of r_p and φ, allowing for the calculation of general helical volumes described in section III.E.

Acknowledgments

This research was carried out independently over the past two years, taking place in both the US and UK. I thank Newton Launch Systems for funding test equipment, Kerax Ltd for wax samples, Addison Place Dental Practice for radiographs, AspireSpace and Richard Newlands for their continued support, Martin Heywood, for providing machining equipment, advising and tea, Samuel Norman and Rob Sandford for supplying a much needed DAQ system, John Barber for procuring a test site, and the invaluable test crew: David James Wright, Ethan Holmes, and Michael Castle. In addition, Greg A. Voth, Stephen A. Whitmore, and Francis W. Starr, for preliminary advising and encouragement. Finally, Ali M. Ahmed, Andrew Ringham and Malcolm Tisdale, who motivated this research in its beginning stages.

References

1. Altman, D., and Holzman, A. "Overview and History of Hybrid Rocket Propulsion," *Fundamentals of Hybrid Rocket Combustion and Propulsion*. American Institute of Aeronautics and Astronautics, 2007, pp. 1-36. doi: 10.2514/5.9781600866876.0001.0036
2. Whitmore, S. A., Armstrong, I. W., Heiner, M. C., and Martinez, C. J. "High-Performing Hydrogen Peroxide Hybrid Rocket with 3-D Printed and Extruded ABS Fuel," *2018 Joint Propulsion Conference*. American Institute of Aeronautics and Astronautics, 2018. doi: 10.2514/6.2018-4443
3. Whitmore, S. A., and Bulcher, A. M. "Vacuum Test of a Novel Green-Propellant Thruster for Small Spacecraft," *53rd AIAA/SAE/ASEE Joint Propulsion Conference*. American Institute of Aeronautics and Astronautics, 2017. doi: 10.2514/6.2017-5044
4. Mechentel, F. S., Coates, A. M., and Cantwell, B. J. "Small-scale Gaseous Oxygen Hybrd Rocket Testing for Regression Rate and Combustion Efficiency Studies," *53rd AIAA/SAE/ASEE Joint Propulsion Conference*. American Institute of Aeronautics and Astronautics, 2017. doi: 10.2514/6.2017-4643
5. Karp, A. C., Nakazono, B., Vaughan, D. A., Story, G. T., Oglesby, B., and Prince, A. "Update on Technology Development Plan for a Low Temperature Hybrid Mars Ascent Vehicle Concept," *2018 Joint Propulsion Conference*. American Institute of Aeronautics and Astronautics, 2018. doi: 10.2514/6.2018-4834
6. Paccagnella, E., Santi, M., Ruffin, A., Barato, F., Pavarin, D., Misté, G. A., Venturelli, G., and Bellomo, N. "Testing of a Long-Burning-Time Paraffin-Based Hybrid Rocket Motor," *Journal of Propulsion and Power*, 2018, pp. 1-11. doi: 10.2514/1.B37144
7. Karabeyoglu, A., Stevens, J., Geyzel, D., Cantwell, B., and Micheletti, D. "High Performance Hybrid Upper Stage Motor," *47th AIAA/ASME/SAE/ASEE Joint Propulsion Conference & Exhibit*. American Institute of Aeronautics and Astronautics, 2011. doi: 10.2514/6.2011-6025
8. Benhidjeb-Carayon, A., Gabl, J., and Pourpoint, T. L. "Hypergolic Ignition and Relights of a Paraffin-based Hybrid Grain," *2018 Joint Propulsion Conference*. American Institute of Aeronautics and Astronautics, 2018. doi: 10.2514/6.2018-4661
9. Lyne, J. E., Brigham, A., Savery, R., Karcher, K., Pyron, J., Adams, L., Reagan, G., Furches, H., Sola, D., and Melendez, L. "The Use of a 3-D Printed, Polymer Matrix Containing Pulverized Fuel in a Hybrid Rocket," *2018 Joint Propulsion Conference*. American Institute of Aeronautics and Astronautics, 2018. doi: 10.2514/6.2018-4597
10. Whitmore, S., Peterson, Z., and Eilers, S. "Analytical and Experimental Comparisons of HTPB and ABS as Hybrid Rocket Fuels," *47th AIAA/ASME/SAE/ASEE Joint Propulsion Conference & Exhibit*. American Institute of Aeronautics and Astronautics, 2011. doi: 10.2514/6.2011-5909
11. Dyrda, D., and Cantwell, B. J. "Development of a Laser Ignition Scheme for Hybrid Rocket Motors," *2018 Joint Propulsion Conference*. American Institute of Aeronautics and Astronautics, 2018. doi: 10.2514/6.2018-4444
12. Sutton, G. P., and Biblarz, O. *Rocket Propulsion Elements*: Wiley, 2016.
13. Karabeyoglu, A., Zilliac, G., Cantwell, B. J., DeZilwa, S., and Castellucci, P. "Scale-Up Tests of High Regression Rate Paraffin-Based Hybrid Rocket Fuels," *Journal of Propulsion and Power* Vol. 20, No. 6, 2004, pp. 1037-1045. doi: 10.2514/1.3340
14. Casillas, E., Shaeffer, C., Trowbridge, J., Casillas, E., Shaeffer, C., and Trowbridge, J. "Cost and performance payoffs inherent in increased fuel regression rates," *33rd Joint Propulsion Conference and Exhibit*. American Institute of Aeronautics and Astronautics, 1997. doi: 10.2514/6.1997-3081
15. Karabeyoglu, M. A., Altman, D., and Cantwell, B. J. "Combustion of Liquefying Hybrid Propellants: Part 1, General Theory," *Journal of Propulsion and Power* Vol. 18, No. 3, 2002, pp. 610-620.

doi: 10.2514/2.5975
16. Whitmore, S. A., Walker, S. D., Merkley, D. P., and Sobbi, M. "High Regression Rate Hybrid Rocket Fuel Grains with Helical Port Structures," *Journal of Propulsion and Power* Vol. 31, No. 6, 2015, pp. 1727-1738. doi: 10.2514/1.B35615
17. McCulley, J., Bath, A., and Whitmore, S. "Design and Testing of FDM Manufactured Paraffin-ABS Hybrid Rocket Motors," *48th AIAA/ASME/SAE/ASEE Joint Propulsion Conference & Exhibit*. American Institute of Aeronautics and Astronautics, 2012. doi: 10.2514/6.2012-3962
18. Armold, D. M., Boyer, J. E., McKnight, B., Kuo, K., Desain, J., Brady, B. B., Fuller, J., and Curtiss, T. J. "Testing of Hybrid Rocket Fuel Grains at Elevated Temperatures with Swirl Patterns Fabricated Using Rapid Prototyping Technology," *50th AIAA/ASME/SAE/ASEE Joint Propulsion Conference*. American Institute of Aeronautics and Astronautics, 2014. doi: 10.2514/6.2014-3754
19. Masato, D., Sorgato, M., and Lucchetta, G. *Prototyping and modeling of the centrifugal casting process for paraffin waxes*, 2017. doi: 10.1080/10426914.2017.1317791
20. Geneviève, B. "Development of a hybrid sounding rocket motor," *Mechanical Engineering*. Vol. Masters, University of Kwazulu-Natal, 2013, p. 191.
21. Carmicino, C., and Sorge, A. R. "Performance comparison between two different injector configurations in a hybrid rocket," *Aerospace Science and Technology* Vol. 11, No. 1, 2007, pp. 61-67. doi: 10.1016/j.ast.2006.08.009
22. Piscitelli, F., Saccone, G., Gianvito, A., Cosentino, G., and Mazzola, L. "Characterization and manufacturing of a paraffin wax as fuel for hybrid rockets," *Propulsion and Power Research* Vol. 7, No. 3, 2018, pp. 218-230. doi: 10.1016/j.jppr.2018.07.007
23. Roberts, J. D., and Caserio, M. C. *Basic principles of organic chemistry*: WA Benjamin, Inc., 1977. doi: 10.2514/5.9781600866876.0001.0036
24. Wernimont, E. J., and Heister, S. D. "Reconstruction Technique for Reducing Hybrid-Rocket Combustion Test Data," *Journal of Propulsion and Power* Vol. 15, No. 1, 1999, pp. 128-136. doi: 10.2514/2.5401
25. Kumar, R., and Ramakrishna, P. A. "Measurement of regression rate in hybrid rocket using combustion chamber pressure," *Acta Astronautica* Vol. 103, 2014, pp. 226-234. doi: 10.1016/j.actaastro.2014.06.044
26. Saito, Y., Kamps, L. T., Komizu, K., Bianchi, D., Nasuti, F., and Nagata, H. "The Accuracy of Reconstruction Techniques for Determining Hybrid Rocket Fuel Regression Rate," *2018 Joint Propulsion Conference*. American Institute of Aeronautics and Astronautics, 2018. doi: 10.2514/6.2018-4923
27. Karabeyoglu, M. A., Cantwell, B. J., and Zilliac, G. "Development of Scalable Space-Time Averaged Regression Rate Expressions for Hybrid Rockets," *Journal of Propulsion and Power* Vol. 23, No. 4, 2007, pp. 737-747. doi: 10.2514/6.2018-4530
28. Story, G. T., Prince, A., Chaffin, J., Kibbey, T. P., Oglesby, B., and Karp, A. C. "Low Temperature Hybrid Mars Ascent Vehicle Concept Development and Planning at MSFC," *2018 Joint Propulsion Conference*. American Institute of Aeronautics and Astronautics, 2018. doi: 10.2514/6.2018-4836
29. Armold, D., Boyer, J. E., Kuo, K., Fuller, J. K., Desain, J., and Curtiss, T. J. "Test of Hybrid Rocket Fuel Grains with Swirl Patterns Fabricated Using Rapid Prototyping Technology," *49th AIAA/ASME/SAE/ASEE Joint Propulsion Conference*. American Institute of Aeronautics and Astronautics, 2013. doi: 10.2514/6.2013-4141
30. Hitt, M. A. "Preliminary Additively Manufactured Axial-Injection, End-Burning Hybrid Rocket Motor Regression Rate Study," *2018 Joint Propulsion Conference*. American Institute of Aeronautics and Astronautics, 2018. doi: 10.2514/6.2018-4598
31. Nagata, H., Teraki, H., Saito, Y., Kanai, R., Yasukochi, H., Wakita, M., and Totani, T. "Verification Firings of End-Burning Type Hybrid Rockets," *Journal of Propulsion and Power* Vol. 33, No. 6, 2017, pp. 1473-1477. doi: 10.2514/1.B36359